

High resolution Ordovician (Floian-Sandbian) carbon isotope stratigraphy from the Jiangnan slope, South China: The first complete record of the MDICE in $\delta^{13}\text{C}_{\text{org}}$ and its global significance

Xiaocong Luan ^{a,*}, Mikael Calner ^b, Fangyi Gong ^a, Oliver Lehnert ^c, Guanzhou Yan ^a, Yuchen Zhang ^a, Zhutong Zhang ^d, Rongchang Wu ^{a,*}

^a State Key Laboratory of Palaeobiology and Stratigraphy, Nanjing Institute of Geology and Palaeontology, Chinese Academy of Sciences, Nanjing 210008, China

^b Department of Geology, Lund University, Sölvegatan 12, SE-223 62 Lund, Sweden

^c GeoZentrum Nordbayern, Friedrich-Alexander Universität Erlangen-Nürnberg (FAU), Schlossgarten 5, D-91054 Erlangen, Germany

^d State Key Laboratory of Lithospheric Evolution, Institute of Geology and Geophysics, Chinese Academy of Sciences, Beijing 100029, China

ARTICLE INFO

Editor: Dr. Bing Shen

Keywords:
 $\delta^{13}\text{C}_{\text{org}}$ chemostratigraphy
MDICE
South China
Black shale
Paleoenvironment
GOBE

ABSTRACT

The Middle Darriwilian Isotopic Carbon Excursion (MDICE) is one of the globally recognized positive excursions in carbon isotope chemostratigraphy, but mainly documented by $\delta^{13}\text{C}_{\text{carb}}$ data in previous research. In this paper, new stable organic carbon isotope data ($\delta^{13}\text{C}_{\text{org}}$) are presented from the Hule-1 core from the southern Anhui Province of southern China. The core constitutes an Ordovician siliciclastic succession deposited in the upper Jiangnan slope. The Ordovician graptolite biostratigraphy of this area is already well established, and ranges from the *Baltograptus deflexus* Zone (Floian) to the *Nemagraptus gracilis* Zone (Sandbian). Based on the well-constructed graptolite biostratigraphy, a low-amplitude positive excursion of middle–late Darriwilian age within the Hulo Formation is confidently identified as the MDICE. The excursion has an amplitude of ca. 1.1‰ starting from the value of -28.0‰ near the base of this formation, reaching a peak at -26.9‰ in the middle, and decreasing to -28.5‰ in its upper part. Therefore, it reveals to our knowledge the globally best preserved and most complete $\delta^{13}\text{C}_{\text{org}}$ record of MDICE hitherto. Our data elucidate the stratigraphic significance of the MDICE also in deeper depositional environments and as a tool for correlation across different lithofacies belts. The inferred perturbation of the global carbon cycle during this time interval was presumably more pronounced than previously thought, confirming that the Darriwilian was a critical time slice in terms of environmental and biosphere changes.

1. Introduction

Over the last few decades, $\delta^{13}\text{C}_{\text{carb}}$ chemostratigraphy has repeatedly proven to be a very useful tool for stratigraphic correlation. In particular, short-lived positive or negative data anomalies, also known as shifts or excursions, are useful for correlation of thin stratigraphic units between widely separated areas (e.g., Kennett, 1982; Johnston et al., 2012; Saltzman and Thomas, 2012; Albanesi et al., 2013; Metzger et al., 2014; Bergström et al., 2020). In comparison to carbonate-based $\delta^{13}\text{C}_{\text{carb}}$ representing marine dissolved inorganic carbon, $\delta^{13}\text{C}_{\text{org}}$ recorded in marine organic matter has similar potential and significance (Kump and Arthur, 1999; Saltzman and Thomas, 2012; Mackensen and Schmiedl, 2019), although their signals are often asynchronous and the latter show

typically shorter stratigraphic range and/or smaller amplitude. In addition to stratigraphic correlation, both systems reflect perturbations in the global carbon cycle, making them valuable for understanding carbon cycling and climate in geological history.

The Middle Darriwilian Isotopic Carbon Excursion (MDICE) is a well-defined, low-amplitude, transient positive carbon isotope excursion of middle–late Darriwilian age (Middle Ordovician). It has been identified in Baltica, Laurentia, Siberia, Argentina Precordillera, Tarim, and North China (Martma, 2005; Albanesi et al., 2013; Calner et al., 2014; Lehnert et al., 2014; Ainsaar et al., 2015, 2020; Albanesi and Ortega, 2016; Zhang and Munnecke, 2016; Wu et al., 2017; Bang and Lee, 2020; Bergström et al., 2020; Goldman et al., 2020; Jing et al., 2022), as well as in South China (Schmitz et al., 2010; Ma et al., 2015; Zhang et al., 2019;

* Corresponding authors.

E-mail addresses: xcluan@nigpas.ac.cn (X. Luan), rcwu@nigpas.ac.cn (R. Wu).

Gong et al., 2021, 2024). These studies, however, have focused on $\delta^{13}\text{C}_{\text{carb}}$ data mainly, while only minor or even no corresponding signals were previously recognized in $\delta^{13}\text{C}_{\text{org}}$ data (e.g., Zhang et al., 2010; Edwards and Saltzman, 2016; Bergström et al., 2018; Zhang et al., 2022). This limited use of chemostratigraphic applications in shale facies, impedes a deeper understanding of the MDICE and the Darriwilian Age, which represent a critical transition interval in both climate and biosphere during the Ordovician (Rasmussen et al., 2016; Trubovitz and Stigall, 2016; Stigall et al., 2019; Luan et al., 2025).

Recently, the Hule-1 drillcore was recovered from near the Hule Town of the southern Anhui Province. The core constitutes an upper Lower–Upper Ordovician sedimentary succession formed on the upper Jiangnan slope of the South China block and consists of mainly siliciclastic rocks and subordinate argillaceous limestone. The well-documented biostratigraphic framework in this area and the well-preserved shale of this core facilitate establishment of a $\delta^{13}\text{C}_{\text{org}}$ chemostratigraphy for the succession. Here we present new high-resolution $\delta^{13}\text{C}_{\text{org}}$ isotopic compositions along with total organic carbon (TOC) content, from the Ningkuo, Hulo, and basal Yenwashan formations of the core. This study documents a complete and biostratigraphically well-constrained MDICE based on $\delta^{13}\text{C}_{\text{org}}$ data and will (1) facilitate correlation based on carbon isotope chemostratigraphy between different lithofacies and areas, and (2) provide new insights into the influences of environmental factors on the MDICE and its linkage to changes in marine biodiversity.

2. Geological setting and stratigraphy

2.1. Geological setting

During the Ordovician Period (485–444 Ma), South China was an independent paleoplate rifted off from Eastern Gondwana (Fig. 1; Torsvik and Cocks, 2013, 2017). The continent formed during the collision between the Yangtze and Cathaysia blocks around 860–820 Ma (Shu et al., 2021), and paleogeographically includes the Yangtze, Jiangnan, and Zhujiang regions during the late Precambrian and early Paleozoic (Chen and Rong, 1992; Zhou et al., 2008). These three paleogeographical regions reflect a gradual transition from the shallow platform, through the slope to the basin areas (Chen and Rong, 1992; Chen et al., 1995). Thus, the Jiangnan region constitutes the slope area connecting the Yangtze epeiric sea to the open ocean.

The Hule-1 core is located in the eastern Jiangnan region (present-day orientation), which represents the upper (proximal) portion of the slope that was adjacent to the platform area and characterized by mixed carbonate-siliciclastic sediments within the studied time interval (Fig. 1). The core was drilled in the year of 2021 at Hule Town, Ningguo City, Anhui Province (GPS, E 30°21'45.2688", N 118°46'13.6567"),

which is 4.5 km north of the Jiangjunling section (Gong et al., 2010; Dong et al., 2018) and 1.6 km northwest of the Xijinhe section (Fang et al., 2024; Liu et al., 2025; the Jinxiqiao and Xiakengwu sections in Wang et al., 1992) (Fig. 2). The tectonic influence on the succession is relatively low, without significant folding or faulting, facilitating the high recovery percentage of this core. The core reaches a total depth of 580 m and comprises, in ascending order, the Tanchiachiao, Ningkuo, Hulo, Yenwashan, Huangnekang, and Xinling formations (all dipping ~20°–30° northwestward).

2.2. Stratigraphy

The Tanchiachiao Formation (aka. Tanjiaqiao Formation) was named at Tanjiaqiao, south of Taiping County, Anhui Province (Hsü, 1936; Sheng, 1974), and is characterized by green, grayish-green, bluish-gray calcareous shale and shale containing limestone concretions. Although the synonymy of this unit with the Yinchufu Formation was proposed by some researchers (Gao et al., 2014b), the usage of Tanchiachiao Formation has been kept at the Jiangjunling section, where several informal members were identified, including a ca. 20-m-thick basal argillaceous limestone, a 186-m-thick lower member of shale, a 157-m-thick middle member of mainly carbonaceous shale, and a 171-m-thick upper member of shale interbedded with nodular limestone (Dong et al., 2018). The trilobite *Asaphopsis-Basilicus* Biozone is documented at the top of this formation in this area (Fig. 3) (Gong et al., 2010).

The Ningkuo Formation (aka. Ningguo Formation) conformably overlies the Tanchiachiao Formation. It was defined in the Huangge–Lanniu areas in Hule Town, Ningguo City, Anhui Province (Hsü, 1934). The typical lithology is a graptolite-rich grayish-green, darkish blue and grayish black shale. At the Xijinhe section (Fang et al., 2024), this formation consists of a lower gray-black silty shale and an upper, dark carbonaceous shale of ca. 180 m and ca. 45 m thickness, respectively. The lithology and thickness is comparable with that of the Ningkuo Formation at the Jiangjunling section, which includes four graptolites biozones *Baltograptus deflexus*, *Azygograptus suecicus*, *Cardiograptus amplus* and *Levisograptus austrodentatus*, in ascending order (Gong et al., 2010).

The Hulo Formation (aka. Hule Formation) was established by Hsü (1934) in the same type locality as the Ningkuo Formation. This formation is characterized by the development of siliceous shale conformably overlying, and distinct from, the Ningkuo Formation (Gao et al., 2014a). It is ca. 50 m in thickness at the Xijinhe section (Fang et al., 2024). Although the upper part of the Hulo Formation is not exposed at the Jiangjunling section, six graptolite biozones were identified in the Hule area, including the *Acrograptus ellesae*, *Nicholsonograptus fasciculatus* and *Pterograptus elegans/Didymograptus*

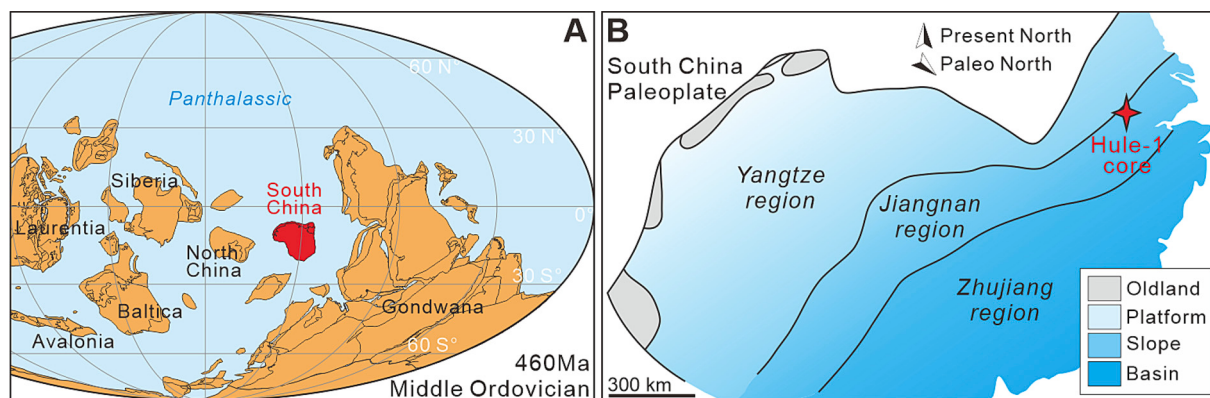


Fig. 1. Paleogeographic location of the Hule-1 core in the Jiangnan region, South China. (A) Paleogeographic reconstruction showing the location of the South China Paleoplate during the Middle Ordovician (ca. 460 Ma). Base map modified from Torsvik and Cocks (2013); (B) Regions of South China during the Ordovician after Zhou et al. (2008).

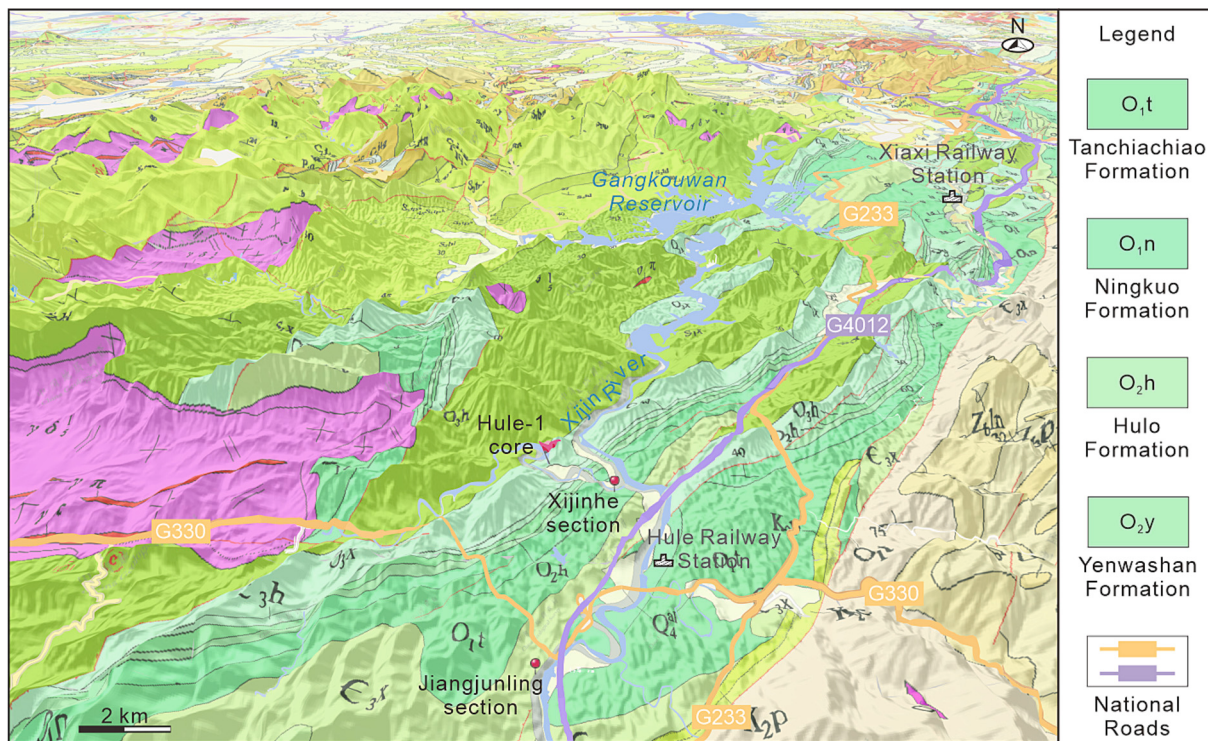


Fig. 2. Geological map showing the locations of the Hule-1 core and selected published sections (Jiangjunling and Xixinhe). The topographical map is exaggerated for visualization (not to scale) and provided by the National Platform for Common GeoSpatial Information Services (tianditu.gov.cn); geology data after GeoCloud (geocloud.cgs.gov.cn). Note only related legends are indicated.

murchisoni biozones in the lower part of the formation, and *D. jiangxiensis*/Hustedograptus teretiusculus/Glossograptus hincksi, Nemagraptus gracilis and Dicranograptus sinensis biozones from the upper part (Qian et al., 1964; Gong et al., 2010; Dong et al., 2018). The successive graptolite biozones ranging from *L. austrodentatus* (uppermost Ningkuo Formation) to *D. sinensis* (uppermost Hulo Formation) were recognized at the Xixinhe section (Wang et al., 1992).

The Yenwashan Formation (aka. Yanwashan Formation) was named in Jiangshan City, Zhejiang Province (Liu and Chao, 1927), referring to a unit of nodular limestone (Gao et al., 2014b). Gong et al. (2010) divided this formation into a lower gray, medium- to thick-bedded calcareous shale, conformably overlying the Hulo Formation, and an upper nodular limestone. The lower part, however, was restricted to the Meishuxia section in the Hule area (Gong et al., 2010). The presence of distinct nodular limestone is the main criteria for recognition of this formation.

The Huangnekang Formation (aka. Huangnigang Formation) is a mainly yellowish green calcareous shale with lime nodules that originally was established in the Jiangshan City area, Zhejiang Province. The overlying Xinling Formation constitutes grayish yellow-green shale, siltstone and sandstone and was formally defined in the Hule County, Anhui Province (Gao et al., 2014a, 2014b). These two formations of Upper Ordovician are the youngest strata of the Hule-1 core. The Xinling, Huangnekang and Yenwashan formations are in conformable contact with each other (Gong et al., 2010).

Based on biostratigraphy, the strata of the Hule-1 core range from uppermost Lower through Upper Ordovician. Only the succession spanning the uppermost Tanchiachiao, through the Ningkuo and Hulo to the lowermost Yenwashan formations, which occupy the 580–280 m interval of the core, was investigated in this study (Fig. 4).

3. Methods

Gamma Ray (GR) measurements were obtained using the SKH-3000 logging instrument, with a natural gamma sampling interval of 0.05 m

and a logging speed of 8 m/min. A total of 39 rock samples and 308 geochemical samples were collected from the studied interval. Thin sections were prepared for rock samples and studied using a polarizing microscope with CCD imaging system (ZEISS Scope A1 equipped with AxioCam 503). Geochemical samples were grinded to 200 meshes for $\delta^{13}\text{C}_{\text{org}}$ and TOC contents analysis.

Splits of ca. 5 g powder per sample were placed in polypropylene tubes, and then decarbonated with 3% (v/v) HCl for 24 h. These samples were centrifuged, and the supernatant was removed. The residual powders were rinsed with Milli-Q water following a stepwise washing procedure and then dried at 70 °C in an oven. After crushed and loaded into capsules, dry samples were flash combusted at 1060 °C in an Organic Elemental Analyzer (FLASH, 2000) fitted with a zero blank autosampler. The TOC contents (wt%) were obtained by a thermal conductivity detector from the resulting CO₂ gas that would be transferred by continuous flow for determination of $\delta^{13}\text{C}$ values (‰, in relative to the Vienna PeeDee Belemnite) on a Delta V Advantage Isotope Ratio Mass Spectrometer at the Nanjing Institute of Geology and Palaeontology. Reproducibility was monitored by replicate analyses with standard error of 0.06‰, and calibration of $\delta^{13}\text{C}$ values was accomplished using a working standard B2151 ($\delta^{13}\text{C}_{\text{org}} = -26.3\text{\textperthousand}$), GBW04407 (black carbon, $\delta^{13}\text{C}_{\text{org}} = -22.4\text{\textperthousand}$) and UREA ($\delta^{13}\text{C}_{\text{org}} = -39.8\text{\textperthousand}$).

4. Results

4.1. Stratigraphy and lithology of the Hule-1 core

A continuous succession through the uppermost Tanchiachiao, Ningkuo, Hulo, to lowermost Yenwashan formations of the Hule-1 core was investigated in this study (Fig. 4). The uppermost Tanchiachiao Formation ranges from 580 m to 573.9 m in the core and is composed of nodular and argillaceous limestone (Fig. 4A) and calcareous shale. The presence of limestone is typical for the Tanchiachiao Formation and its

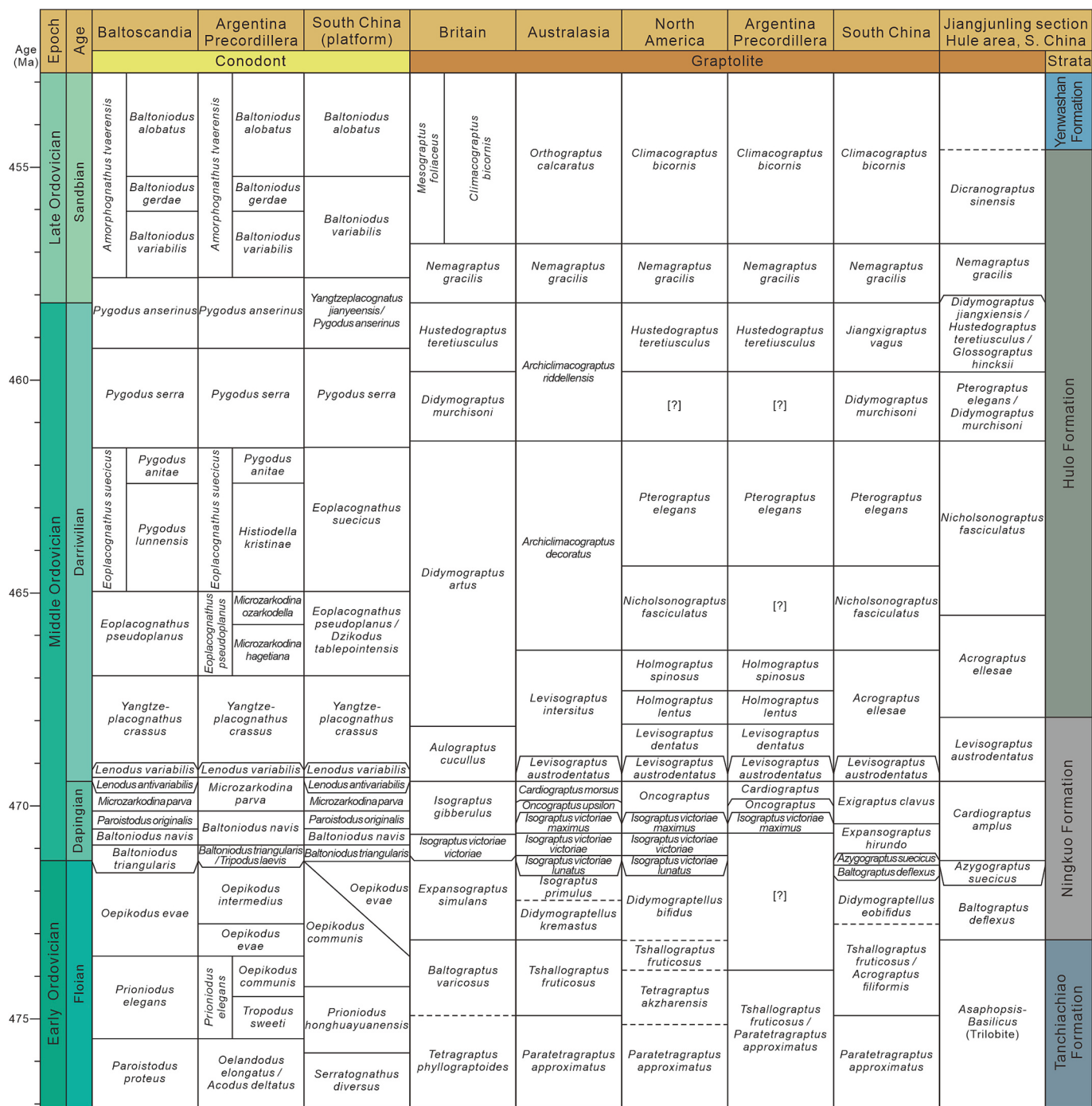


Fig. 3. Chronostratigraphic framework and global biostratigraphic correlation of biozones documented from the study area. The biostratigraphy of the Jiangjunling section is based on Gong et al. (2010) and Dong et al. (2018), and the global biozonations are adapted from Goldman et al. (2023) and references therein.

disappearance at ca. 573.9 m marks the base of the Ningkuo Formation. The lowermost interval (573.9–573.3 m) of the latter formation is composed of siliceous shale (Fig. 5A), while the remainder of the lower parts of the formation (573.3–469.4 m) is mainly shale with a few interbeds of calcareous shale (Figs. 4B, 5B). By contrast, the upper part of the Ningkuo Formation (469.4–392.8 m) is characterized by carbonaceous shale and siltstone (Figs. 4C–E, 5C). Accordingly, the lithology of Ningkuo Formation in the Hule-1 core coincides well with the lithological development at the Jiangjunling and Xijinhe sections.

The re-appearance of siliceous shale at 392.8 m marks the base of the Hulo Formation (Figs. 4F, 5D). In the lower portion of the formation, this siliceous shale is interbedded with carbonaceous shale (392.8–374.9 m).

The majority of the formation (374.9–305.5 m), however, is characterized by a continuous succession of siliceous shale (Figs. 4G, 5E), resulting in relatively poor core integrity. The uppermost part of the Hulo Formation (305.5–287.1 m) is typified by carbonaceous shale and calcareous shale (Fig. 4H, 5F), and may correspond to the lowermost Yenwashan Formation at the Meishuxia section, as described by Gong et al. (2010). However, the transition from continuous siliceous shale to interbedded carbonaceous shale–calcareous shale in the upper Hulo Formation is not as distinct as the appearance of nodular limestone slightly higher up in the core section (Fig. 5I), making the base of the latter a better boundary between the Hulo and Yenwashan formations in the Hule-1 core.

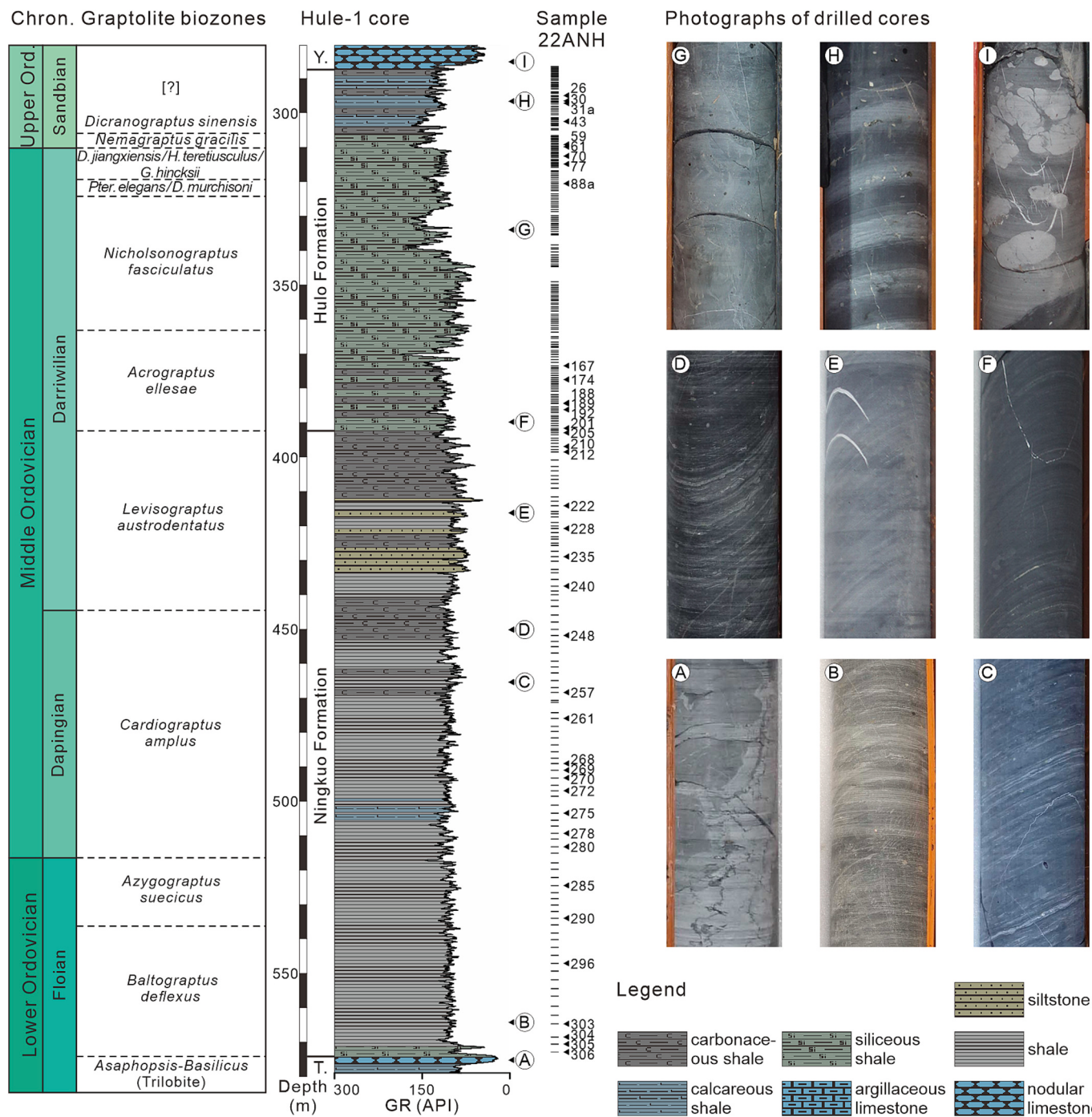


Fig. 4. Stratigraphy of the Lower–Upper Ordovician succession in the Hule-1 core. (A) Nodular or mottled limestone; (B) parallel laminated shale; (C) wavy laminated shale; (D) wavy laminated carbonaceous shale; (E) very thinly bedded siltstone to silty shale, with calcite veins perpendicular to bedding plane; (F) thinly bedded siliceous shale; (G) thin to medium bedded siliceous shale; (H) calcareous shale–carbonaceous shale couplets, with abundant pyrite; (I) nodular limestone. All cores are 8 cm in diameter. Age assignments are based on lithological comparison to the nearby, biostratigraphically controlled Jiangjunling section (Gong et al., 2010; Dong et al., 2018; Fang et al., 2024). Sampling levels including rock samples for thin sections are prefixed as 22ANH. Abbreviations: T., Tanchiachiao Formation; Y., Yenwashan Formation.

Gamma Ray (GR) logs of the Hule-1 core provide additional understanding of lithological changes and trends within the studied interval (Fig. 4). The average GR values from the limestone and carbonaceous shale of the Tanchiachiao Formation are 33 and 88 API, respectively. The shale of the Ningkuo Formation has GR values in the range of 87–105 API, whereas the siltstone of this formation has GR values in the range of 58–85 API. The GR values of the siliceous shale of the Hulo Formation average around 115 API, which is distinct from the 56 API of

the Yenwashan limestone in average. The GR values reflect the lithology and aid to recognize formation boundaries, as revealed by the higher natural radioactivity in the Ningkuo and Hulo formations due to higher contents of siliciclastic clay and organic matter.

4.2. TOC content and $\delta^{13}\text{C}_{\text{org}}$ record

Stratigraphic variations in TOC content are relatively minor in the

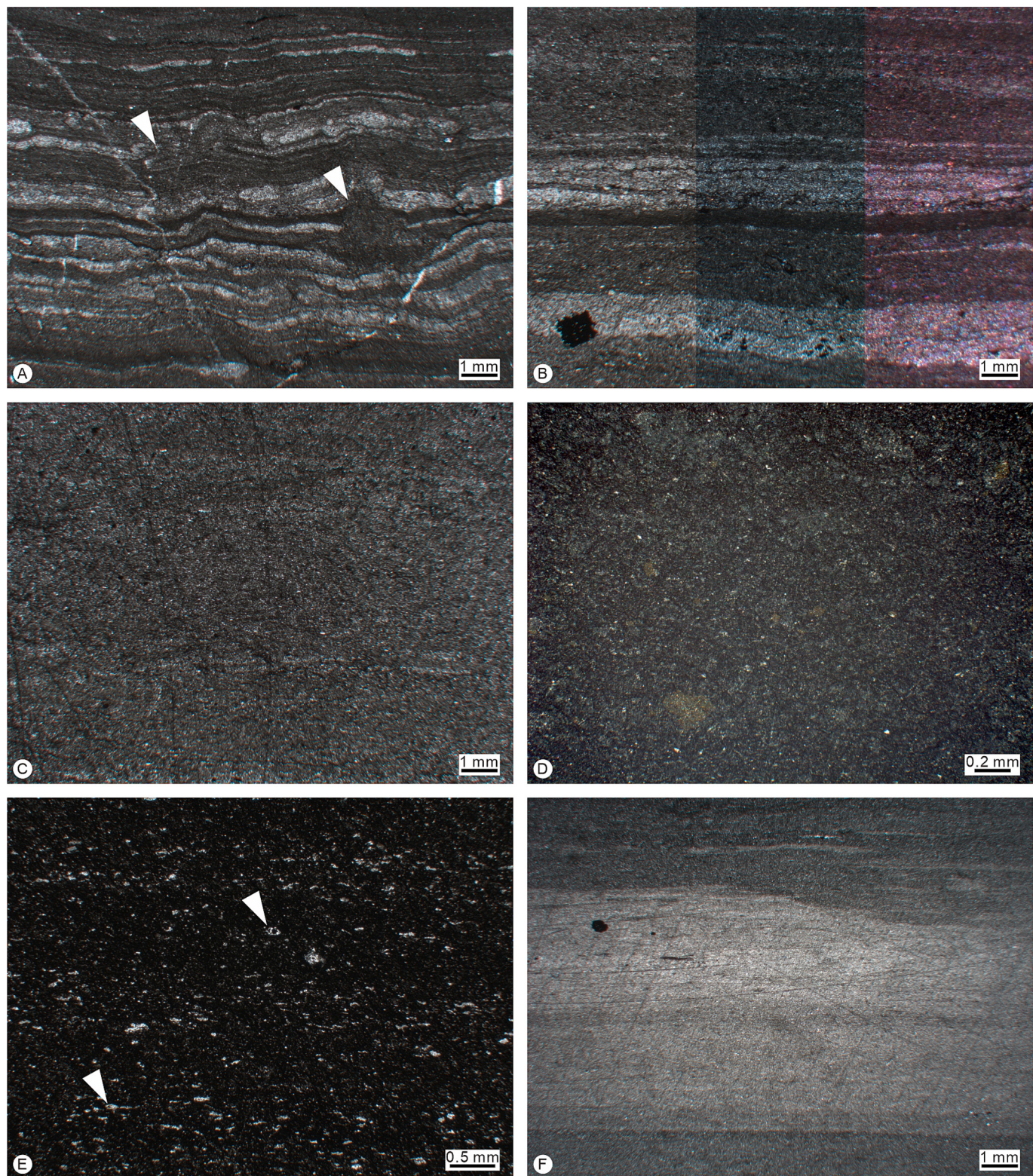


Fig. 5. Photomicrographs of the Ningkuo and Hulo formations in the Hule-1 core. (A) laminated siliceous shale of the Ningkuo Fm., note burrows cutting the laminae (white arrows), under plane polarized light, Sample No. 22ANH305; (B) shale of the Ningkuo Fm., showing alternating quartzose and clayey layers, under plane polarized light, cross polarized light and cross polarized light with gypsum plate from left to right, Sample No. 22ANH280; (C) silty shale of the Ningkuo Fm., under plane polarized light, Sample No. 22ANH235; (D) siliceous shale of the Hulo Fm., goldenish pyrites under reflected light, Sample No. 22ANH167; (E) siliceous shale of the Hulo Fm., abundant carbonaceous content, containing radiolarians (white arrows), under plane polarized light, Sample No. 22ANH077; (F) interbedded calcareous shale of the Hulo Fm., under plane polarized light, Sample No. 22ANH031a.

Ningkuo Formation, in which the average value is 0.64 wt% ($n = 103$) but ranging from 0.15 to 2.00 wt% (Fig. 6). The average TOC content value obtained from the Hulo Formation is 3.52 wt% ($n = 200$) with a gradually increasing trend from ca. 2 wt% to ca. 4 wt% in the lower and middle parts, showing relatively high values, with peak values over 12 wt% in the upper part. A few TOC content values of the basal Yenwashan Formation show an average around 4.36 wt% ($n = 5$), excluding a data point of 2.75 wt% corresponding to an outlier of paired $\delta^{13}\text{C}_{\text{org}}$ as discussed below.

The $\delta^{13}\text{C}_{\text{org}}$ values from Ningkuo Formation show considerable scattering around an average value of $-26.6\text{\textperthousand}$. The values show an overall upward decrease through the formation, from ca. $-25.3\text{\textperthousand}$ to ca. $-27.8\text{\textperthousand}$. By contrast, the consistency of values from Hulo Formation is very high, with an average value of $-27.2\text{\textperthousand}$. A small but distinct jump

in the values around ca. 390 m, where the rock is relatively fractured, is possibly due to a minor discontinuity. Apart from that, a continuously, distinctly positive excursion of ca. $1.1\text{\textperthousand}$ is recorded; starting at a value of $-28.0\text{\textperthousand}$ near the base of Hulo Formation and reaching a peak value of $-26.9\text{\textperthousand}$ in the middle part of the formation. Values thereafter decrease gradually through the middle and upper parts of the formation to reach a distinct low at $-28.5\text{\textperthousand}$ around 15 m below the top of the formation. In the uppermost portion, the $\delta^{13}\text{C}_{\text{org}}$ values rise again, continuously to the top of the studied core succession, at the base of Yenwashan Formation, in which an outlier of $-19.0\text{\textperthousand}$ has been excluded from the data set.

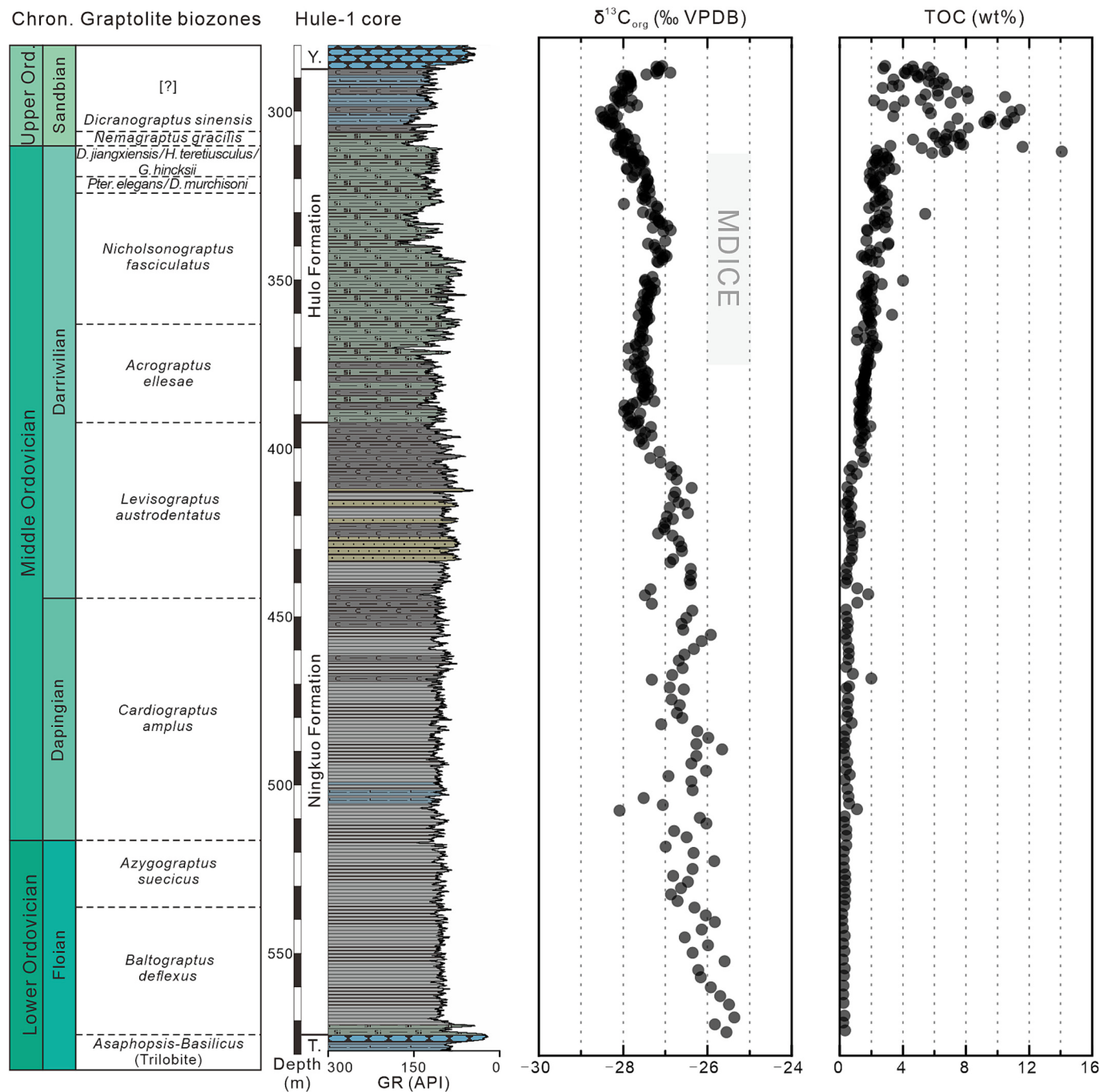


Fig. 6. $\delta^{13}\text{C}_{\text{org}}$ record and TOC content in the Hule-1 core.

5. Discussion

5.1. Evaluation of the $\delta^{13}\text{C}_{\text{org}}$ data

Temporal trends and excursions in $\delta^{13}\text{C}_{\text{carb}}$, representing marine dissolved inorganic carbon (DIC) incorporated in the marine carbonate, have proved to be very useful for stratigraphic correlation of limestone successions (Kennett, 1982; Johnston et al., 2012; Saltzman and Thomas, 2012; Metzger et al., 2014; Bergström et al., 2020). Similarly, $\delta^{13}\text{C}$ excursions recorded from marine organic matter ($\delta^{13}\text{C}_{\text{org}}$), controlled by marine algae utilizing the DIC pool (Mackensen and Schmiedl, 2019), can be measured from organic-rich rocks and thus is a potentially important complement for stratigraphic correlation of the fine-grained siliciclastic sedimentary rocks. Direct comparison of the two systems, however, is complicated, as the precise timing and amplitude of excursions may vary between $\delta^{13}\text{C}_{\text{org}}$ and $\delta^{13}\text{C}_{\text{carb}}$ (Saltzman and Thomas, 2012, and references therein). This is because the $\delta^{13}\text{C}_{\text{org}}$ signals are influenced by biological offset in carbon fixation, local source of organic carbon and different diagenetic pathways (Kump and Arthur, 1999; Metzger et al., 2014). Generally, the parallel trends of $\delta^{13}\text{C}_{\text{org}}$ and $\delta^{13}\text{C}_{\text{carb}}$ in stratigraphic intervals characterized by significant disturbances in the carbon cycle, still suggest a potential for stratigraphic correlation (Saltzman and Thomas, 2012), as exemplified by the Hirnantian positive Isotopic Carbon Excursion of the Late Ordovician (Underwood et al., 1997; Brenchley et al., 2003; Zhang et al., 2009; Melchin et al., 2017; Bergström et al., 2020; Hints et al., 2023).

There is a ca. 7% difference in composition between terrestrial and marine organic matter due to land plant photosynthesis (Mackensen and Schmiedl, 2019), and their rise and widespread colonization around Late Ordovician might have impacted the marine realm during that time (Servais et al., 2019; Yuan et al., 2023). Therefore, the potential influences of terrestrial contamination need to be considered as $\delta^{13}\text{C}_{\text{org}}$ is more susceptible at low TOC contents (Johnston et al., 2012). A threshold of 0.5 wt% of TOC content in the rock has been proposed, and proved to be useful (Wang et al., 2017; Zhao et al., 2021). In the Ningkuo Formation, the TOC content is low, with a mean value of 0.64 wt%, while much higher contents are recorded in the Hule (avg. 3.52 wt%) and Yenwashan (avg. 4.36 wt%) formations (Fig. 6). Accordingly, the $\delta^{13}\text{C}_{\text{org}}$ data from the Hule and Yenwashan formations seem to represent more reliable records than those from the Ningkuo Formation.

Diagenetic alteration also needs to be checked before applying $\delta^{13}\text{C}_{\text{org}}$ data to stratigraphic correlation, for which covariations between $\delta^{13}\text{C}_{\text{org}}$ and TOC content can serve as indicators (Zhang et al., 2009; Metzger et al., 2014; Hints et al., 2023). Either increase or decrease in $\delta^{13}\text{C}_{\text{org}}$ values is reasonable along with diagenetic degradation of organic matter in sediments (Freudenthal et al., 2001), therefore organic carbon isotopic excursions controlled by diagenetic alteration can be ruled out only if there is a lack of correlation between $\delta^{13}\text{C}_{\text{org}}$ and TOC content. A moderate fit of the linear regression to the data from Ningkuo Formation ($R^2 = 0.64$, Fig. 7) suggests minor negative correlation between $\delta^{13}\text{C}_{\text{org}}$ and TOC content, which is consistent with the diagenetic degradation of TOC resulting in positive shift of $\delta^{13}\text{C}_{\text{org}}$ values in sediments, following the Rayleigh-fractionation model. By contrast, quite poor fits of linear regression to the data from Hule ($R^2 = 0.47$) and Yenwashan ($R^2 = 0.38$) formations infer no significant correlations, indicating those are reliable records of a primary signal.

5.2. Correlation of the MDICE in $\delta^{13}\text{C}_{\text{org}}$ and $\delta^{13}\text{C}_{\text{carb}}$ records

5.2.1. Biostratigraphically constrained $\delta^{13}\text{C}_{\text{org}}$ data from the Hule-1 core

A detailed biostratigraphic framework (Fig. 3) has been established for the sedimentary succession in the Hule area based on studies at the Jiangjunling section and sections in the Huangge–Lanniwu area (Hsü, 1934; Gong et al., 2010). The Tanchiachiao Formation includes the graptolite *Dictyonema*–*Bryograptus* Biozone and the *Clonograptus flexilis taipingensis* Biozone (Qian et al., 1964; Gong et al., 2010). There are four

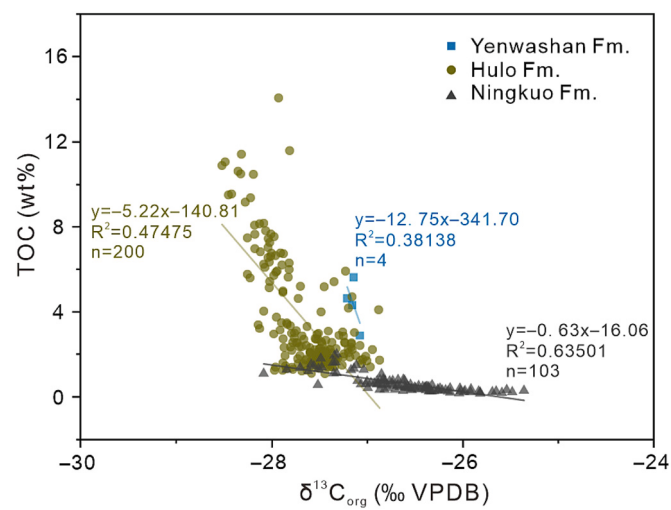


Fig. 7. Cross-plot and linear fits of $\delta^{13}\text{C}_{\text{org}}$ versus TOC content from the Hule-1 core.

graptolite biozones documented from the Ningkuo Formation, including the *Baltograptus deflexus*, *Azygograptus suecicus*, *Cardiograptus amplus*, and *Levisograptus austrodentatus* biozones, in ascending order (Qian et al., 1964; Gong et al., 2010). The lower portion of the Hule Formation includes the *Didymograptus ellesae*, *Nicholsonograptus fasciculatus* and *Pterograptus elegans*/*Didymograptus murchisoni* biozones, whereas the *Didymograptus jiangxiensis*/*Hustedograptus teretiusculus*, *Nemagraptus gracilis* and *Dicranograptus sinensis* biozones occur in the upper Hule Formation (Gong et al., 2010). Hence, based on the graptolite biostratigraphy established in the adjacent outcrops, the $\delta^{13}\text{C}_{\text{org}}$ data from the Hule-1 core can be assigned as ranging from Floian (late Early Ordovician) to Sandbian (early Late Ordovician) in age (Fig. 6).

In the Ningkuo Formation, the $\delta^{13}\text{C}_{\text{org}}$ values exhibit a general decrease from ca. -25.3 to -27.8‰ spanning the *Baltograptus deflexus*, *Azygograptus suecicus*, *Cardiograptus amplus* and *Levisograptus austrodentatus* biozones of late Floian to early Darriwilian age. In the lower part of the *Acrograptus ellesae* Biozone of the Hule Formation, the $\delta^{13}\text{C}_{\text{org}}$ values increase shortly from ca. -28.0 to -27.3‰, then decrease to -27.9‰. This trend is followed by a transient but prominent positive $\delta^{13}\text{C}_{\text{org}}$ shift from -28.0‰ (in the *Acrograptus ellesae* Biozone) to a maximum of -26.87‰ (in the *Nicholsonograptus fasciculatus* Biozone). Upwards from the peak, the $\delta^{13}\text{C}_{\text{org}}$ values decrease continuously throughout the *Pterograptus elegans*/*Didymograptus murchisoni* and the *D. jiangxiensis*/*Hustedograptus teretiusculus*/*Glossograptus hincksi* biozones, to a distinct low, with values of -28.5‰ above the *Nemagraptus gracilis* Biozone. Above that level, the $\delta^{13}\text{C}_{\text{org}}$ values rise again.

Based on the age of the biostratigraphic zonation (Goldman et al., 2023), the $\delta^{13}\text{C}_{\text{org}}$ record presented herein can be tied to global chronostratigraphy (Figs. 6 and 8). The steady decrease in $\delta^{13}\text{C}_{\text{org}}$ values through the Ningkuo Formation ranges through the Floian, Dapingian and into the lower Darriwilian. The data shows relatively large scatter and is accompanied by low TOC content that appears to reflect a very small increase in accumulation of organic material upwards through the formation (Fig. 6). As mentioned in Section 5.1, however, the reliability of the $\delta^{13}\text{C}_{\text{org}}$ data from this part of the succession may be low and data should be used for stratigraphic correlation with caution. By contrast, the $\delta^{13}\text{C}_{\text{org}}$ data from the overlying Hule Formation shows very little scatter in $\delta^{13}\text{C}_{\text{org}}$ values and may well preserve a primary isotopic signal, ranging from lower Darriwilian to upper Sandbian. These data show good consistency with a better potential for stratigraphic correlation. The long transient shift in $\delta^{13}\text{C}_{\text{org}}$, with an amplitude of approximately +1.1‰, is of middle–late Darriwilian age and can, therefore, confidently be interpreted as the Middle Darriwilian Isotope Carbon Excursion (MDICE). It is notable that the rate of increase in TOC accelerates in the

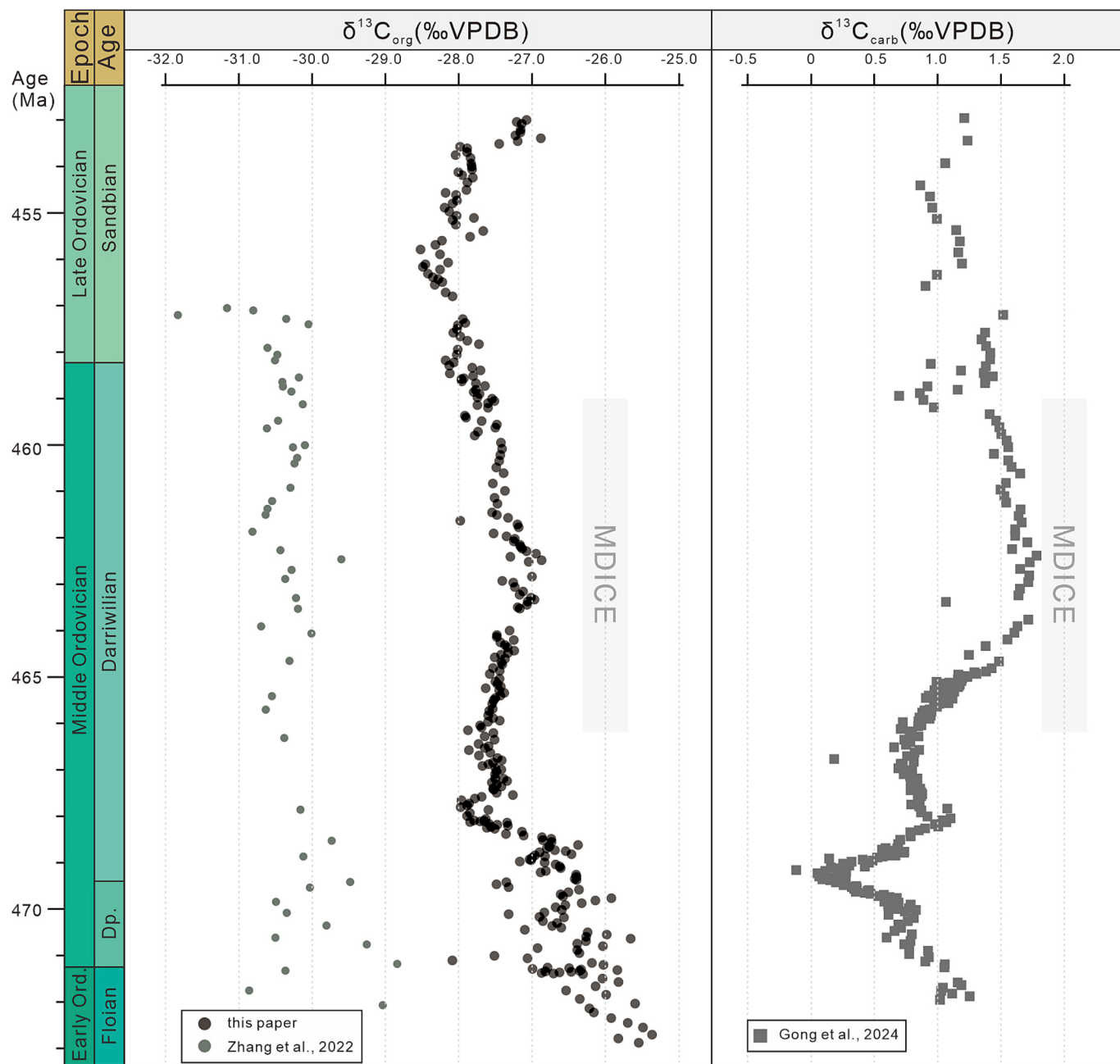


Fig. 8. Correlation of $\delta^{13}\text{C}_{\text{org}}$ data between the Hule-1 core, Anhui Province (this paper), and the Anye-1 core, Zhejiang Province (Zhang et al., 2022), with $\delta^{13}\text{C}_{\text{carb}}$ data from the Shidi-1 core, Hunan Province (Gong et al., 2024). Note the difference in amplitude of the MDICE indicated by gray bands between the two isotopic systems.

corresponding interval, until the end of the MDICE, where a facies change occurs and a strong increase in TOC are recorded directly above (Fig. 6).

5.2.2. Regional and global correlation of the MDICE

The MDICE is not only the earliest major carbon isotopic excursion during the Middle–Late Ordovician, but represents an unusually long-lasting event, being documented from numerous paleoplates, i.e., Baltica, Siberia, Laurentia, Argentina Precordillera, Tarim, North China and South China (Ainsaar et al., 2010; Schmitz et al., 2010; Munnecke et al., 2011; Albanesi et al., 2013; Calner et al., 2014; Lehnert et al., 2014; Ainsaar et al., 2015, 2020; Albanesi and Ortega, 2016; Zhang and Munnecke, 2016; Saltzman and Edwards, 2017; Wu et al., 2017; Bang and Lee, 2020; Gong et al., 2021, 2024; Jing et al., 2022). To date, the

MDICE was defined and observed in $\delta^{13}\text{C}_{\text{carb}}$ data from marine carbonate deposits. Although a corresponding excursion has been documented in published $\delta^{13}\text{C}_{\text{org}}$ records (Bergström et al., 2020), a complete and well preserved $\delta^{13}\text{C}_{\text{org}}$ MDICE has so far not been published (e.g., Zhang et al., 2010; Edwards and Saltzman, 2016). Hence, the herein documented record from the Hulo Formation will become an important new addition as it is unusually well-preserved and supported by biostratigraphy.

In South China, several previous studies suggested that only the rising limb of the MDICE is preserved in $\delta^{13}\text{C}_{\text{carb}}$ data due to an upper Darriwilian sedimentary hiatus cutting off the peak interval and the falling limb of this chemostratigraphic event (Schmitz et al., 2010; Munnecke et al., 2011; Gong et al., 2021). This view, however, is becoming more complex following a recent study on the Shidi-1 core by

Gong et al. (2024). The Shidi-1 core succession is obviously more complete as the lithological units formed in the most distal zone on the Yangtze platform area, at the transition to the Jiangnan slope. This is likely the reason that this $\delta^{13}\text{C}_{\text{carb}}$ study (Gong et al., 2024) documented a complete MDICE (Fig. 8) within the *Dzikodus tablepointensis* Biozone (rising limb), the *Eoplacoganthus suecicus* Biozone (peak values), and the *Pygodus serra* Biozone (falling limb), all conodont zones of early-middle to late Darriwilian age (Fig. 3). The Shidi-1 core excursion, with an amplitude of ca. 1‰ and a peak of ca. 1.7‰, may thus serve as a $\delta^{13}\text{C}_{\text{carb}}$ reference section of South China for intercontinental correlation. In terms of $\delta^{13}\text{C}_{\text{org}}$ records, the MDICE is not documented in the Yangtze region (platform area) (Zhang et al., 2010), whereas its existence has been confirmed and supported by graptolite biozones in the Anye-1 core, Jiangnan region (slope area) (Zhang et al., 2022), although that record is of lower sampling resolution and with a less clear positive shift (Fig. 8). The Hule-1 core also represents the Jiangnan slope area, and preserves a comparable $\delta^{13}\text{C}_{\text{org}}$ record to that of Anye-1 core, but with a far more complete record of the MDICE containing a clear rising limb, a peak interval, and a falling limb. Despite there is an approximately 2.5% difference in baseline values between the two records, their similar trends support that the $\delta^{13}\text{C}_{\text{org}}$ data reflect similar changes along the Jiangnan slope area. More importantly, the trend of the MDICE in the $\delta^{13}\text{C}_{\text{org}}$ record from the Hule-1 core, synchronously correlates with that in the Shidi-1 core (Fig. 8), underlining the potential for stratigraphic correlation by means of $\delta^{13}\text{C}_{\text{org}}$ records.

In Baltica, the MDICE in $\delta^{13}\text{C}_{\text{carb}}$ ranges from the *Eoplacognathus pseudoplanus* to the *P. anserinus* Conodont Biozone (Ainsaar et al., 2010,

2020; Lehnert et al., 2014; Wu et al., 2017), with peak values of 1–2.5% (1–2‰ above baseline values). The corresponding $\delta^{13}\text{C}_{\text{org}}$ shift on Baltica rises only <0.5‰ above baseline values and ranges from the *Nicholsonograptus fasciculatus* to the *Pseudoplexograptus distichus* Graptolite Biozone (Bergström et al., 2018; Bergström et al., 2020). Although there is a good age correspondence between the two isotope systems, the relatively subtle shift in $\delta^{13}\text{C}_{\text{org}}$ weakens its usage for comparative correlation (Fig. 9). In addition, the MDICE is a global event that can be recognized from $\delta^{13}\text{C}_{\text{carb}}$ data on several paleocontinents (Ainsaar et al., 2020; Bergström et al., 2020 and references therein), whereas a limited numbers of previous studies on $\delta^{13}\text{C}_{\text{org}}$ records suggest no corresponding shifts, such as those on Laurentia (Edwards and Saltzman, 2016) and in the Yangtze region (platform) of South China (Zhang et al., 2010). The data presented in this study, however, exhibit a prominent and well-preserved corresponding MDICE of ca. 1.1‰. This implies a more profound environmental significance of this excursion than previously believed and warrants more study on offshore sedimentary successions and integration of graptolite and conodont chronostratigraphies.

5.3. Significance for paleoenvironment and biosphere

The Darriwilian Age represents a particularly interesting time interval for investigating and understanding co-evolution of global climate and marine biodiversity (Fig. 10). This time interval is associated with the onset of a proposed Gondwana glaciation (Rasmussen et al., 2016, 2021; Albanesi et al., 2020), and oceanic-atmospheric general circulation models have suggested the emergence and expansion of a south

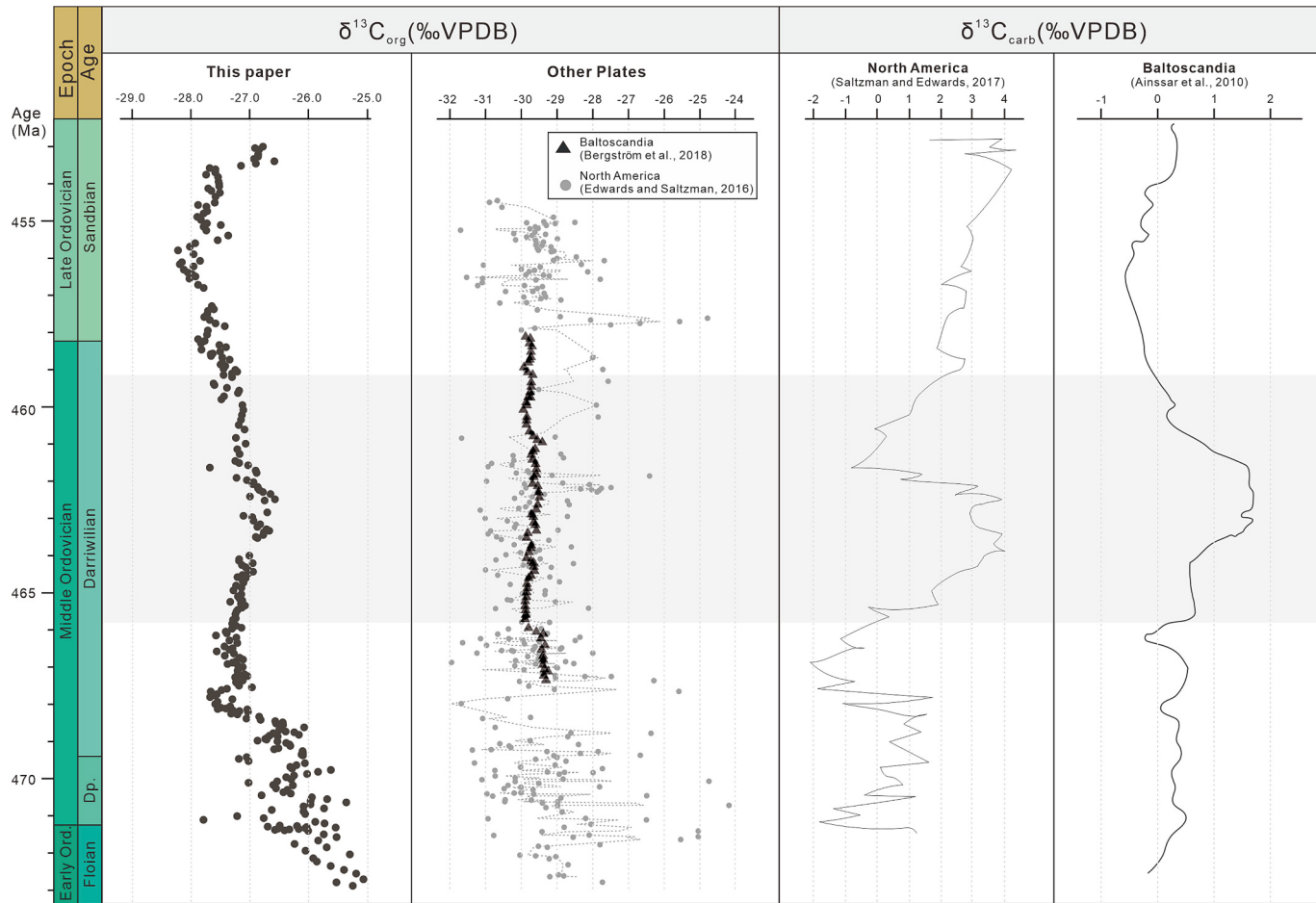


Fig. 9. Global correlation of the $\delta^{13}\text{C}_{\text{org}}$ record from the Hule-1 core, South China, with $\delta^{13}\text{C}_{\text{org}}$ data from Baltoscandia (Bergström et al., 2018) and North America (Edwards and Saltzman, 2016), and with $\delta^{13}\text{C}_{\text{carb}}$ data from Baltoscandia (Ainsaar et al., 2010) and North America (Saltzman and Edwards, 2017).

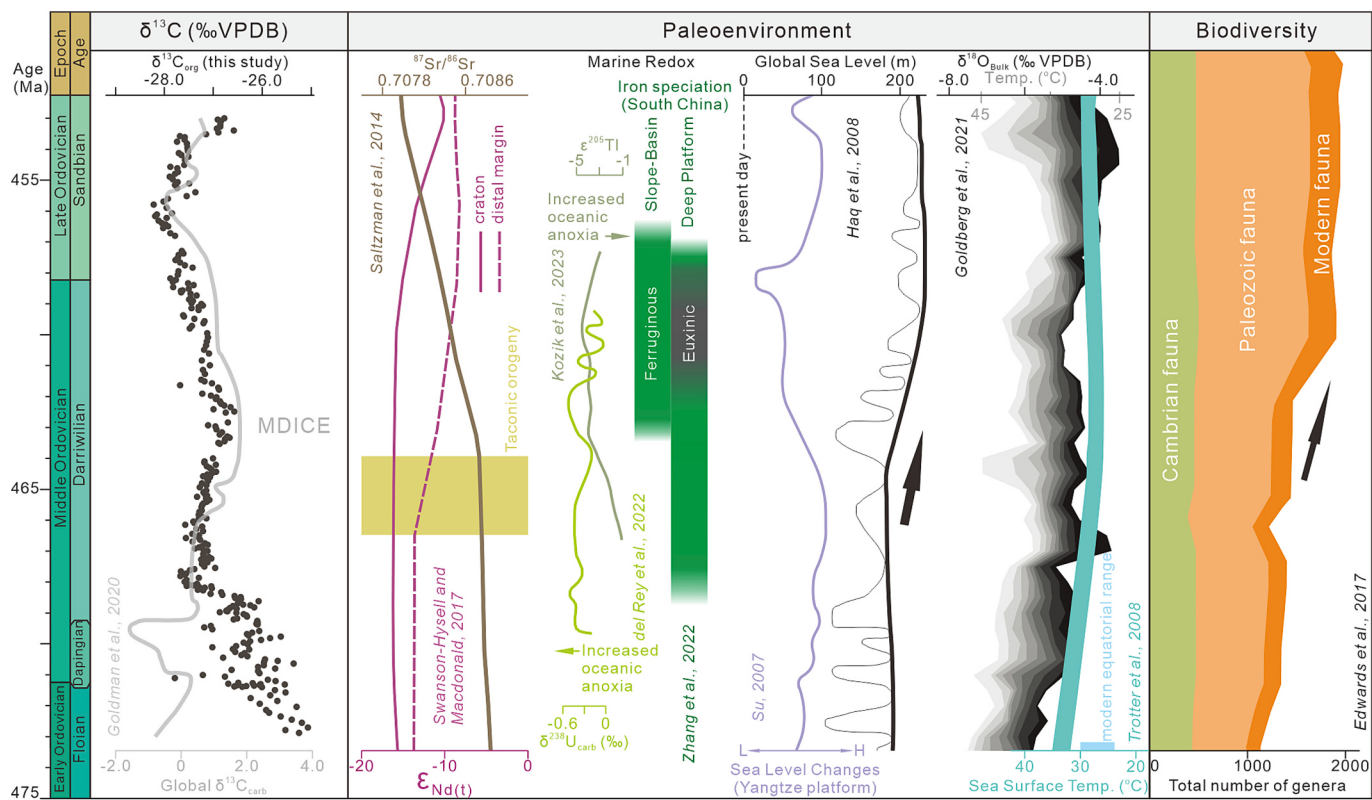


Fig. 10. Summary chronostratigraphic chart of the studied part of the Hule-1 core. The left panel shows the new $\delta^{13}\text{C}_{\text{org}}$ record, with comparison to the compiled global $\delta^{13}\text{C}_{\text{carb}}$ trend. The right panel shows significant paleoenvironmental and biological changes during the corresponding late Early–early Late Ordovician time interval (del Rey et al., 2022; Goldberg et al., 2021; Su, 2007).

polar ice sheet around this time (Pohl et al., 2014, 2016; Luan et al., 2025). This time was also characterized by improved atmospheric and oceanic oxygenation (Edwards et al., 2017; Kozik et al., 2023), enhanced silicate weathering (Young et al., 2009; Swanson-Hysell and Macdonald, 2017; Conwell et al., 2022), a superplume event (Barnes, 2004), an increase of micrometeorite dust (Schmitz et al., 2008; Schmitz et al., 2019) and/or the formation of a dust ring around the Earth (Tomkins et al., 2024). More importantly, the most significant biodiversification during Phanerozoic Era, known as the Great Ordovician Biodiversification Event (GOBE), reached a global biodiversity peak during this time interval (Trubovitz and Stigall, 2016; Stigall et al., 2019), although it has also been argued this biodiversity peak was part of a prolonged radiation rather than an isolated event (Servais and Harper, 2018; Servais et al., 2023). The MDICE is thus an important chemostratigraphic tool, not only for defining time and for comparison of environmental changes (or forcing) in different settings, but may also assist in interpreting processes across these settings.

Using the MDICE as a target interval and considering its likely origin as enhanced organic burial, the associated negative shift in $\delta^{34}\text{S}_{\text{CAS}}$ has been, instead of microbial sulfate reduction and enhanced continental weathering, probably controlled by reduced rates of microbially mediated pyrite burial and organic matter remineralization linked to marine oxygenation and progressive ventilation (Young et al., 2016). This oxygenation pulse is also inferred directly from both local and global redox proxies (Kozik et al., 2023), despite it might be also accompanied by expansion of anoxic sea-water due to intensified circulation (Zhang et al., 2022, 2024). However, this view is challenged by the cyclostratigraphic study of the MDICE interval by Ren et al. (2023) that infers overall marine anoxia during this time. Moreover, links between the MDICE and climate have also been discussed, arguing that the increase of the $\delta^{13}\text{C}$ values may correlate to a burst in primary production facilitated by global cooling and better ventilation, thus, reflecting the

trigger for the GOBE (Trotter et al., 2008; Rasmussen et al., 2016), despite a worldwide rise in sea-level has been proposed (Haq and Schutter, 2008). It is noteworthy that these scenarios are in contradiction with each other or are not based on direct comparisons with the MDICE.

Naturally, the reliability and origin of the MDICE could be vital to reconstruct paleoenvironment. The line of evidence implies that this isotopic excursion is global, which is supported by an independent strontium isotope stratigraphic correlation (Saltzman et al., 2014; Saltzman and Edwards, 2017). Besides, recent research on calcium isotopes reveals the preservation of the MDICE as a primary signal (Adiatma et al., 2024). To date, most researchers agreed that this positive shift in $\delta^{13}\text{C}$ might be caused by an elevated primary productivity resulting in an enhanced burial of organic matter (Rasmussen et al., 2016; Wu et al., 2017; Jing et al., 2022). There are still many remaining questions on its origins requiring more detailed investigations in future. For instance, Bang and Lee (2020) proposed that the MDICE developed due to a local response to global transgression, resulting from anti-estuarine circulation and consequent organic carbon burial in an isolated basin environment. Regarding its unusually long-lasting duration, Ainsaar et al. (2020) suggested the MDICE should be of more complex origins, rather than a simple response to global cooling or sea-level rise.

The MDICE, as identified in $\delta^{13}\text{C}_{\text{org}}$ records from the Hule-1 core, presumably indicates a perturbation in the global carbon cycle, revealed by the most distinct positive shift reported yet. The MDICE based on $\delta^{13}\text{C}_{\text{org}}$ is most likely controlled by global factors, since a good connectivity to open marine conditions in South China is suggested by a comparable record in both isotopic systems, in the $\delta^{13}\text{C}_{\text{carb}}$ (Gong et al., 2024) as well as in the $\delta^{13}\text{C}_{\text{org}}$ records (this study). Besides the significance for stratigraphic correlation, the $\delta^{13}\text{C}_{\text{org}}$ trends observed herein have potentials and implications in respect to the paleoenvironment. The black shale, now with a well-documented $\delta^{13}\text{C}_{\text{org}}$ signal may serve

as a future archive for multidisciplinary research, providing new insights into the understanding of the evolving environment and biosphere during this critical transitional interval.

6. Conclusion

This study presents a highly time-resolved set of $\delta^{13}\text{C}_{\text{org}}$ data coupled with data on TOC content, of fine-grained, siliciclastic-rich rocks from the Ningkuo, Hulo and basal Yenwashan formations in the recently drilled Hule-1 core, southern Anhui Province, South China. The studied part of the core spans the upper Floian to the Sandbian stages and paleogeographically represents the Jiangnan slope.

The $\delta^{13}\text{C}_{\text{org}}$ data in the Ningkuo and Hulo formations show an overall trend that is comparable to published records from South China and other paleoplates. A transient but distinct positive excursion of middle–late Darriwilian age is documented in the Hulo Formation and can, based on biostratigraphy, be recognized as a complete record of the Middle Darriwilian Isotopic Carbon Excursion (MDICE). The recent discovery of a complete $\delta^{13}\text{C}_{\text{carb}}$ record of the MDICE from the nearby shallow-marine platform area plus our complete $\delta^{13}\text{C}_{\text{org}}$ record of MDICE from the Jiangnan slope changes the traditional view that due to a sedimentary hiatus, only the rising limb of this important chemostratigraphic marker is preserved in South China. Instead, our study reveals one of the most complete MDICE records based on $\delta^{13}\text{C}_{\text{org}}$ data to date, including a rising limb, peak interval and a falling limb. It not only provides a representative $\delta^{13}\text{C}_{\text{org}}$ curve facilitating stratigraphic correlation across different lithofacies belts, but also infers that this positive excursion resulted from a perturbation in the global carbon cycle. The black shale of the Hulo Formation, preserving a complete record of the MDICE, may thus serve as an archive for future research that may provide new insights into Darriwilian significant paleoenvironmental and ecosystem changes.

CRediT authorship contribution statement

Xiaocong Luan: Writing – review & editing, Writing – original draft, Visualization, Validation, Supervision, Software, Resources, Project administration, Methodology, Investigation, Formal analysis, Data curation, Conceptualization. **Mikael Calner:** Writing – review & editing, Writing – original draft, Validation, Methodology, Investigation. **Fangyi Gong:** Writing – review & editing, Visualization, Methodology, Investigation, Formal analysis, Data curation. **Oliver Lehnert:** Writing – review & editing, Writing – original draft, Validation, Methodology, Investigation. **Guanzhou Yan:** Writing – review & editing, Data curation. **Yuchen Zhang:** Writing – review & editing, Data curation. **Zhutong Zhang:** Writing – review & editing, Data curation. **Rongchang Wu:** Writing – review & editing, Writing – original draft, Project administration, Methodology, Investigation, Funding acquisition, Conceptualization.

Declaration of competing interest

The authors declare that they have no known competing financial interests or personal relationships that could have appeared to influence the work reported in this paper.

Acknowledgements

Beneficial discussions with Renbin Zhan, Junpeng Zhang and Lixia Li are sincerely acknowledged. Field and lab assistances were provided by Xiaole Zhang, Jianfeng Liu, Chenguang Zhang, Mingshuai Xu, Yucheng Wang, Xinle Zhang, Hongyong Zhang and Jing Liu. Constructive comments and editings from Guillermo L. Albanesi, Andrej Spiridonov and Bing Shen are greatly appreciated. This study was funded by the Strategic Priority Research Program of the Chinese Academy of Sciences (XDB08500000), and the National Natural Science Foundation of China

(42572130, 42102130). OL was supported by the Deutsche Forschungsgemeinschaft (Le 867/13-1 and 13-2). This is a contribution to IGCP 735, “Rocks and the Rise of Ordovician Life – Filling Knowledge Gaps in the Early Palaeozoic Biodiversification”.

Appendix A. Supplementary data

Supplementary data to this article can be found online at <https://doi.org/10.1016/j.palaeo.2025.113227>.

Data availability

The authors confirm that all data necessary for supporting the scientific findings of this paper have been provided.

References

- Adiatma, Y.D., Saltzman, M.R., Griffith, E.M., 2024. Calcium isotope constraints on a Middle Ordovician carbon isotope excursion. *Earth Planet. Sci. Lett.* 641, 118805.
- Ainsaar, L., Kaljo, D., Martma, T., Meidla, T., Männik, P., Nõlvak, J., Tinn, O., 2010. Middle and Upper Ordovician carbon isotope chemostratigraphy in Baltoscandia: a correlation standard and clues to environmental history. *Palaeogeogr. Palaeoclimatol. Palaeoecol.* 294, 189–201.
- Ainsaar, L., Männik, P., Dronov, A.V., Izokh, O.P., Meidla, T., Tinn, O., 2015. Carbon isotope chemostratigraphy and conodonts of the Middle–Upper Ordovician succession in the Tungus Basin, Siberian Craton. *Palaeoworld* 24, 123–135.
- Ainsaar, L., Dronov, A., Kipli, E., Meidla, T., Radzevicius, S., Tinn, O., 2020. Stratigraphy and facies differences of the Middle Darriwilian Isotopic Carbon Excursion (MDICE) in Baltoscandia. *Estonian J. Earth Sci.* 69, 214–222.
- Albanesi, G.L., Ortega, G., 2016. Conodont and Graptolite Biostratigraphy of the Ordovician System of Argentina. In: Montenari, M. (Ed.), *Stratigraphy & Timescales*. Academic Press, pp. 61–121.
- Albanesi, G.L., Bergström, S.M., Schmitz, B., Serra, F., Feltes, N.A., Voldman, G.G., Ortega, G., 2013. Darriwilian (Middle Ordovician) $\delta^{13}\text{C}_{\text{carb}}$ chemostratigraphy in the Precordillera of Argentina: Documentation of the middle Darriwilian Isotope Carbon Excursion (MDICE) and its use for intercontinental correlation. *Palaeogeogr. Palaeoclimatol. Palaeoecol.* 389, 48–63.
- Albanesi, G.L., Barnes, C.R., Trotter, J.A., Williams, I.S., Bergström, S.M., 2020. Comparative Lower–Middle Ordovician conodont oxygen isotope palaeothermometry of the Argentine Precordillera and Laurentian margins. *Palaeogeogr. Palaeoclimatol. Palaeoecol.* 549, 109115.
- Bang, S., Lee, Y.I., 2020. Darriwilian carbon isotope stratigraphy in the Taebaeksan Basin, Korea and its implications for Middle Ordovician paleoceanography. *Palaeogeogr. Palaeoclimatol. Palaeoecol.* 541, 109534.
- Barnes, C.R., 2004. Was there an Ordovician superlumine event. In: Webby, B.D., Paris, F., Droser, M.L., Percival, I.G. (Eds.), *The Great Ordovician Biodiversification Event*. Columbia University Press, New York, pp. 77–80.
- Bergström, S.M., Ahlberg, P., Maletz, J., Lundberg, F., Joachimski, M.M., 2018. Darriwilian (Middle Ordovician) chemostratigraphy linked to graptolite, conodont and trilobite biostratigraphy in the Fågelsång-3 drill core, Scania, Sweden. *Gff* 140, 229–240.
- Bergström, S.M., Eriksson, M.E., Ahlberg, P., 2020. Chapter six - Ordovician $\delta^{13}\text{C}$ chemostratigraphy: A global review of major excursions and their ties to graptolite and conodont biostratigraphy. In: Montenari, M. (Ed.), *Stratigraphy & Timescales*. Academic Press, pp. 319–351.
- Brenchley, P.J., Carden, G.A., Hints, L., Kaljo, D., Marshall, J.D., Martma, T., Meidla, T., Nõlvak, J., 2003. High-resolution stable isotope stratigraphy of Upper Ordovician sequences: Constraints on the timing of bioevents and environmental changes associated with mass extinction and glaciation. *Geol. Soc. Am. Bull.* 115, 89–104.
- Calner, M., Lehnert, O., Wu, R., Dahlqvist, P., Joachimski, M.M., 2014. $\delta^{13}\text{C}$ chemostratigraphy in the Lower–Middle Ordovician succession of Öland (Sweden) and the global significance of the MDICE. *GFF* 136, 48–54.
- Chen, X., Rong, J., 1992. Ordovician plate tectonics of China and its neighbouring regions. In: Webby, B.D., Laurie, J.R. (Eds.), *Global Perspectives on Ordovician Geology*. Balkema, Rotterdam, pp. 277–291.
- Chen, X., Rong, J., Wang, X., Wang, Z., Zhang, Y., Zhan, R., 1995. Correlation of the Ordovician Rocks of China: Charts and Explanatory Notes. International Union of Geological Sciences Publication, p. 104.
- Conwell, C.T., Saltzman, M.R., Edwards, C.T., Griffith, E.M., Adiatma, Y.D., 2022. Nd isotopic evidence for enhanced mafic weathering leading to Ordovician cooling. *Geology* 50, 886–890.
- del Rey, A., Rasmussen, C.M.Ø., Calner, M., Wu, R., Asael, D., Dahl, T.W., 2022. Stable Ocean redox during the main phase of the Great Ordovician Biodiversification Event. *Commun. Earth & Environ.* 3, 220.
- Dong, Y., Liu, J., Chen, Y., Zhong, S., Zhan, R., 2018. Redox variation during the early and Middle Ordovician in South China and its implication to the Great Ordovician Biodiversification Event. *Acta Sci. Nat. Univ. Pekin.* 54 (4), 739–751 (in Chinese with English abstract).
- Edwards, C.T., Saltzman, M.R., 2016. Paired carbon isotopic analysis of Ordovician bulk carbonate ($\delta^{13}\text{C}_{\text{carb}}$) and organic matter ($\delta^{13}\text{C}_{\text{org}}$) spanning the Great Ordovician Biodiversification Event. *Palaeogeogr. Palaeoclimatol. Palaeoecol.* 458, 102–117.

- Edwards, C.T., Saltzman, M.R., Royer, D.L., Fike, D.A., 2017. Oxygenation as a driver of the Great Ordovician Biodiversification Event. *Nat. Geosci.* 10, 925–929.
- Fang, C., Liu, M., Zhang, C., Tang, H., Li, J., Xing, G., Li, F., Xu, N., Wu, T., Liu, B., 2024. Middle Ordovician climatic and oceanic destabilization in a slope-setting of the Yangtze platform, South China, and its role as a regional brake on the Ordovician radiations. *Palaeogeogr. Palaeoclimatol. Palaeoecol.* 112265.
- Freudenthal, T., Wagner, T., Wenzhöfer, F., Zabel, M., Wefer, G., 2001. Early diagenesis of organic matter from sediments of the eastern subtropical Atlantic: evidence from stable nitrogen and carbon isotopes. *Geochim. Cosmochim. Acta* 65, 1795–1808.
- Gao, Z., Chen, K., Gao, L., 2014a. Dictionary of the Lithostratigraphic Unit of China, Volume 1. University of Electronic Science and Technology of China Press, Chengdu (646 pp (in Chinese)).
- Gao, Z., Chen, K., Gao, L., 2014b. Dictionary of the Lithostratigraphic Unit of China, Volume 2. University of Electronic Science and Technology of China Press, Chengdu (700 pp (in Chinese)).
- Goldberg, S.L., Present, T.M., Finnegan, S., Bergmann, K.D., 2021. A high-resolution record of early Paleozoic climate. *Proc. Natl. Acad. Sci.* 118 e2013083118.
- Goldman, D., Sadler, P.M., Leslie, S.A., Melchin, M.J., Agterberg, F.P., Gradstein, F.M., 2020. Chapter 20 - the Ordovician Period. In: Gradstein, F.M., Ogg, J.G., Schmitz, M.D., Ogg, G.M. (Eds.), *The Geologic Time Scale 2020*. Elsevier, pp. 631–694.
- Goldman, D., Leslie, S., Liang, Y., Bergström, S., 2023. Ordovician Biostratigraphy - Index Fossils, Biozones, and Correlation. *Geol. Soc. Lond. Spec. Publ.* 532, 31–62.
- Gong, W., Qi, D., Bi, Z., Jiang, L., 2010. Restudying the Ordovician System in Hule, Ningguo, Anhui. *Geol. Anhui* 20 (2), 85–89 (in Chinese with English abstract).
- Gong, F., Joachimski, M.M., Yan, G., Li, L., Wei, X., Wu, R., 2021. Middle to late Ordovician carbon isotope chemostratigraphy of the lower Yangtze Platform: Implications for global correlation. *Geol. J.* 56, 2772–2784.
- Gong, F., Luan, X., Calner, M., Lehnert, O., Zhang, Y., Yan, G., Wei, X., Wu, R., 2024. High resolution Ordovician carbon isotope chemostratigraphy in South China and its significance for global correlation. *Glob. Planet. Chang.* 104523.
- Haq, B.U., Schutter, S.R., 2008. A chronology of Paleozoic Sea-level changes. *Science* 322, 64–68.
- Hints, O., Ainsaar, L., Lepland, A., Liiv, M., Männik, P., Meidla, T., Nõlvak, J., Radzevicius, S., 2023. Paired carbon isotope chemostratigraphy across the Ordovician–Silurian boundary in central East Baltic: Regional and global signatures. *Palaeogeogr. Palaeoclimatol. Palaeoecol.* 624, 111640.
- Hsu, S., 1934. The graptolites of the lower Yangtze Valley. Monograph of the National Research Institute of Geology. *Academia Sinica (Series A)* 4, 1–106 (in English with Chinese abstract).
- Hsu, S., 1936. The Tremadocian in South Anhui. *Bull. Geol. Soc. China* 15 (1), 105–108.
- Jing, X., Zhao, Z., Fu, L., Zhang, C., Fan, R., Shen, Y., Yang, B., 2022. Biostratigraphically-controlled Darriwilian (Middle Ordovician) $\delta^{13}\text{C}$ excursions in North China: Implications for correlation and climate change. *Palaeogeogr. Palaeoclimatol. Palaeoecol.* 601, 111149.
- Johnston, D.T., Macdonald, F.A., Gill, B.C., Hoffman, P.F., Schrag, D.P., 2012. Uncovering the Neoproterozoic carbon cycle. *Nature* 483, 320–323.
- Kennett, J.P., 1982. Marine geology. Prentice-Hall, Englewood Cliffs, p. 813.
- Kozik, N.P., Young, S.A., Ahlberg, P., Lindskog, A., Owens, J.D., 2023. Progressive marine oxygenation and climatic cooling at the height of the Great Ordovician Biodiversification Event. *Global Planet. Chang.* 104183.
- Kump, L.R., Arthur, M.A., 1999. Interpreting carbon-isotope excursions: carbonates and organic matter. *Chem. Geol.* 161, 181–198.
- Lehnert, O., Meinhold, G., Wu, R., Calner, M., Joachimski, M.M., 2014. $\delta^{13}\text{C}$ chemostratigraphy in the upper Tremadocian through lower Katian (Ordovician) carbonate succession of the Siljan district, Central Sweden. *Eston. J. Earth Sci.* 63, 277–286.
- Liu, C., Chao, Y., 1927. The Geology of Western Zhejiang. Geological Bulletin of the National Institute of Geological Survey, *Academia Sinica No. 9*, pp. 51–74 (in Chinese).
- Liu, M., Yuan, W., Fang, C., Wang, X., Tan, N., Zhao, M., Wang, X., Algeo, T.J., Sun, P., Feng, X., Chen, D., 2025. Mercury isotope evidence for Middle Ordovician photic-zone euxinia: Implications for termination of the Great Ordovician biodiversification event. *Gondwana Res.* 137, 131–144.
- Luan, X., Sproat, C.D., Jin, J., Pufahl, P.K., Wu, R., Zhan, R., 2025. Upwelling-related ferruginous ooids, microbialites, and the Darriwilian tipping point of Ordovician climate. *Geology*. <https://doi.org/10.1130/G53374.1>.
- Ma, X., Wang, Z.-H., Zhang, Y.-D., Song, Y.-Y., Fang, X., 2015. Carbon isotope records of the Middle–Upper Ordovician transition in Yichang area, South China. *Palaeoworld* 24, 136–148.
- Mackensen, A., Schmidl, G., 2019. Stable carbon isotopes in paleoceanography: atmosphere, oceans, and sediments. *Earth Sci. Rev.* 197, 102893.
- Martma, T., 2005. Ordovician carbon isotopes. In: Poldvere, A. (Ed.), *Mehikoroma* (421) drill core. Estonian geological sections. *Estonian Geological Survey Bulletin*, vol. 6, pp. 25–27.
- Melchin, M.J., Sheets, H.D., Mitchell, C.E., Fan, J., 2017. A new approach to quantifying stratigraphical resolution: application to global stratotypes. *Lethaia* 50, 407–423.
- Metzger, J.G., Fike, D.A., Smith, L.B., 2014. Applying carbon-isotope stratigraphy using well cuttings for high-resolution chemostratigraphic correlation of the subsurface. *AAPG Bull.* 98, 1551–1576.
- Munnecke, A., Zhang, Y., Liu, X., Cheng, J., 2011. Stable carbon isotope stratigraphy in the Ordovician of South China. *Palaeogeogr. Palaeoclimatol. Palaeoecol.* 307, 17–43.
- Pohl, A., Donnadieu, Y., Le Hir, G., Buoncristiani, J.F., Vennin, E., 2014. Effect of the Ordovician paleogeography on the (in)stability of the climate. *Clim. Past* 10, 2053–2066.
- Pohl, A., Donnadieu, Y., Le Hir, G., Ladant, J.B., Dumas, C., Alvarez-Solas, J., Vandenbergroch, T.R.A., 2016. Glacial onset predated late Ordovician climate cooling. *Paleoceanography* 31, 800–821.
- Qian, Y., Li, J., Li, W., Jiang, N., Bi, Z., Gao, Y., 1964 A revision of Sinian and Lower Paleozoic in Southern Anhui, China. In: Chinese Academy of Sciences. *Collected Papers of Nanjing Institute of Geology and Palaeontology*, Chinese Academy of Sciences, Beijing: Science Press, 21–66 (in Chinese).
- Rasmussen, C.M., Ullmann, C.V., Jakobsen, K.G., Lindskog, A., Hansen, J., Hansen, T., Eriksson, M.E., Dronov, A., Frei, R., Korte, C., Nielsen, A.T., Harper, D.A.T., 2016. Onset of main Phanerozoic marine radiation sparked by emerging Mid Ordovician icehouse. *Sci. Rep.* 6, 18884.
- Rasmussen, J.A., Thibault, N., Mac Ørum Rasmussen, C., 2021. Middle Ordovician astrochronology decouples asteroid breakup from glacially-induced biotic radiations. *Nat. Commun.* 12, 6430.
- Ren, C., Fang, Q., Wu, H., Fang, J., Zhang, S., Yang, T., Li, H., 2023. Cyclostratigraphic correlation of Middle–Late Ordovician sedimentary successions between the South China Block and Tarim Basin with paleoclimatic and geochronological implications. *J. Asian Earth Sci.* 246, 105577.
- Saltzman, M.R., Edwards, C.T., 2017. Gradients in the carbon isotopic composition of Ordovician shallow water carbonates: a potential pitfall in estimates of ancient CO₂ and O₂. *Earth Planet. Sci. Lett.* 464, 46–54.
- Saltzman, M.R., Thomas, E., 2012. Chapter 11 - Carbon Isotope Stratigraphy. In: Gradstein, F.M., Ogg, J.G., Schmitz, M.D., Ogg, G.M. (Eds.), *The Geologic Time Scale*. Elsevier, Boston, pp. 207–232.
- Saltzman, M.R., Edwards, C.T., Leslie, S.A., Dwyer, G.S., Bauer, J.A., Repetski, J.E., Harris, A.G., Bergström, S.M., 2014. Calibration of a conodont apatite-based Ordovician 87Sr/86Sr curve to biostratigraphy and geochronology: Implications for stratigraphic resolution. *Geol. Soc. Am. Bull.* 126, 1551–1568.
- Schmitz, B., Harper, D.A.T., Peucker-Ehrenbrink, B., Stouge, S., Almark, C., Cronholm, A., Bergström, S.M., Tassinari, M., Wang, X., 2008. Asteroid breakup linked to the Great Ordovician biodiversification event. *Nat. Geosci.* 1, 49–53.
- Schmitz, B., Bergström, S.M., Wang, X., 2010. The middle Darriwilian (Ordovician) $\delta^{13}\text{C}$ excursion (MDICE) discovered in the Yangtze Platform succession in China: implications of its first recorded occurrences outside Baltoscandia. *J. Geol. Soc. Lond.* 167, 249–259.
- Schmitz, B., Farley, K.A., Goderis, S., Heck, P.R., Bergström, S.M., Boschi, S., Claeys, P., Debaile, V., Dronov, A., van Ginneken, M., Harper, D.A.T., Iqbal, F., Friberg, J., Liao, S., Martin, E., Meier, M.M.M., Peucker-Ehrenbrink, B., Soens, B., Wieler, R., Terfelt, F., 2019. An extraterrestrial trigger for the mid-Ordovician ice age: Dust from the breakup of the L-chondrite parent body. *Science Advances* 5, eaax4184.
- Servais, T., Harper, D.A.T., 2018. The Great Ordovician Biodiversification Event (GOBE): definition, concept and duration. *Lethaia* 51, 151–134.
- Servais, T., Cascales-Miñana, B., Cleal, C.J., Gerrienne, P., Harper, D.A.T., Neumann, M., 2019. Revisiting the Great Ordovician diversification of land plants: recent data and perspectives. *Palaeogeogr. Palaeoclimatol. Palaeoecol.* 534, 109280.
- Servais, T., Cascales-Miñana, B., Harper, D.A.T., Lefebvre, B., Munnecke, A., Wang, W., Zhang, Y., 2023. No (Cambrian) explosion and no (Ordovician) event: a single long-term radiation in the early Palaeozoic. *Palaeogeogr. Palaeoclimatol. Palaeoecol.* 623, 111592.
- Sheng, X., 1974. The Ordovician Subdivision and Correlation of China. Geological Publishing House, Beijing (153 pp (in Chinese)).
- Shu, L., Yao, J., Wang, B., Faure, M., Charvet, J., Chen, Y., 2021. Neoproterozoic plate tectonic process and Phanerozoic geodynamic evolution of the South China Block. *Earth Sci. Rev.* 216, 103596.
- Stigall, A.L., Edwards, C.T., Freeman, R.L., Rasmussen, C.M.O., 2019. Coordinated biotic and abiotic change during the Great Ordovician Biodiversification Event: Darriwilian assembly of early Paleozoic building blocks. *Palaeogeogr. Palaeoclimatol. Palaeoecol.* 530, 249–270.
- Su, W.B., 2007. Ordovician Sea-level changes: evidence from the Yangtze Platform. *Acta Palaeontol. Sin.* 46 (Suppl), 471–476 (in English with Chinese abstract).
- Swanson-Hysell, N.L., Macdonald, F.A., 2017. Tropical weathering of the Taconic orogeny as a driver for Ordovician cooling. *Geology* 45, 719–722.
- Tomkins, A.G., Martin, E.L., Cawood, P.A., 2024. Evidence suggesting that earth had a ring in the Ordovician. *Earth Planet. Sci. Lett.* 646, 118991.
- Torsvik, T.H., Cocks, L.R.M., 2013. New global palaeogeographical reconstructions for the early Palaeozoic and their generation. *Geol. Soc. Lond. Mem.* 38, 5–24.
- Torsvik, T.H., Cocks, L.R.M., 2017. *Earth History and Palaeogeography*. Cambridge University Press, Cambridge, United Kingdom, p. 317.
- Trotter, J.A., Williams, I.S., Barnes, C.R., Lécuyer, C., Nicoll, R.S., 2008. Did Cooling Oceans Trigger Ordovician Biodiversification? Evidence from Conodont Thermometry. *Science* 321, 550–554.
- Trubovitz, S., Stigall, A.L., 2016. Synchronous diversification of Laurentian and Baltic rhynchonelliform brachiopods: Implications for regional versus global triggers of the Great Ordovician Biodiversification Event. *Geology* 44, 743–746.
- Underwood, C.J., Crowley, S.F., Marshall, J.D., Brenchley, P.J., 1997. High-Resolution carbon isotope stratigraphy of the basal Silurian Stratotype (Dob's Linn, Scotland) and its global correlation. *J. Geol. Soc. Lond.* 154, 709–718.
- Wang, H., Yu, J., Bian, L., Feng, H., Fang, Y., 1992. Geochemical study of the early and Middle Ordovician black graptolite shale in the southern Anhui-northern Jiangxi area. *J. Stratigr.* 16 (4), 241–255 (in Chinese with English abstract).
- Wang, W., Guan, C., Zhou, C., Peng, Y., Pratt, L.M., Chen, X., Chen, L., Chen, Z., Yuan, X., Xiao, S., 2017. Integrated carbon, sulfur, and nitrogen isotope chemostratigraphy of the Ediacaran Lantian Formation in South China: Spatial gradient, ocean redox oscillation, and fossil distribution. *Geobiology* 15, 552–571.

- Wu, R., Calner, M., Lehnert, O., 2017. Integrated conodont biostratigraphy and carbon isotope chemostratigraphy in the Lower–Middle Ordovician of southern Sweden reveals a complete record of the MDICE. *Geol. Mag.* 154, 334–353.
- Young, S.A., Gill, B.C., Edwards, C.T., Saltzman, M.R., Leslie, S.A., 2016. Middle–Late Ordovician (Darriwilian–Sandbian) decoupling of global sulfur and carbon cycles: Isotopic evidence from eastern and southern Laurentia. *Palaeogeogr. Palaeoclimatol. Palaeoecol.* 458, 118–132.
- Young, S.A., Saltzman, M.R., Foland, K.A., Linder, J.S., Kump, L.R., 2009. A major drop in seawater $^{87}\text{Sr}/^{86}\text{Sr}$ during the Middle Ordovician (Darriwilian): Links to volcanism and climate? *Geology* 37, 951–954.
- Yuan, W., Liu, M., Chen, D., Xing, Y.W., Spicer, R.A., Chen, J., Them 2nd, T.R., Wang, X., Li, S., Guo, C., Zhang, G., Zhang, L., Zhang, H., Feng, X., 2023. Mercury isotopes show vascular plants had colonized land extensively by the early Silurian. *Sci. Adv.* 9 eade9510.
- Zhang, Y., Munnecke, A., 2016. Ordovician stable carbon isotope stratigraphy in the Tarim Basin, NW China. *Palaeogeogr. Palaeoclimatol. Palaeoecol.* 458, 154–175.
- Zhang, T., Shen, Y., Zhan, R., Shen, S., Chen, X., 2009. Large perturbations of the carbon and sulfur cycle associated with the late Ordovician mass extinction in South China. *Geology* 37, 299–302.
- Zhang, T., Shen, Y., Algeo, T.J., 2010. High-resolution carbon isotopic records from the Ordovician of South China: Links to climatic cooling and the Great Ordovician Biodiversification Event (GOBE). *Palaeogeogr. Palaeoclimatol. Palaeoecol.* 289, 102–112.
- Zhang, Y., Zhan, R., Zhen, Y., Wang, Z., Yuan, W., Fang, X., Ma, X., Zhang, J., 2019. Ordovician integrative stratigraphy and timescale of China. *Sci. China Earth Sci.* 49, 61–88.
- Zhang, J., Li, C., Fang, X., Li, W., Deng, Y., Tu, C., Algeo, T.J., Lyons, T.W., Zhang, Y., 2022. Progressive expansion of seafloor anoxia in the Middle to late Ordovician Yangtze Sea: Implications for concurrent decline of invertebrate diversity. *Earth Planet. Sci. Lett.* 598, 117858.
- Zhang, J., Li, W., Fang, X., Wu, X., Li, C., Zhang, Y., 2024. Marine eutrophication within the Tarim Platform in sync with Middle to late Ordovician climatic cooling. *J. Geol. Soc. Lond.* 181 jgs2023–2078.
- Zhao, X., Wang, W., Xie, G., Pan, S., Jarzembski, E.A., Zheng, D., 2021. Depositional environment of Middle Triassic organic-rich shales in the Ordos Basin, Northwest China. *Geol. J.* 56, 4849–4860.
- Zhou, Z., Zhen, Y., Zhou, Z., Yuan, W., 2008. Division of the Ordovician geographic units of China — a synopsis. *J. Palaeogeogr.* 10 (2), 175–182 (in English with Chinese abstract).